Effect of Annealing Temperature on Structural and, Morphological Properties of Zno Thins Films

Moustafa Debbab (mus.debbab@gmail.com)
Abou Bekr Belkaid University Tlemcen: Universite Abou Bekr Belkaid Tlemcen
Nassera Ghellai
Université Abou Baker Belkaid
Meymoun Belaoui
Université Abou Baker Belkaid
Chafiaa Yaddadene
Centre de Recherche en Technologie des Semi-conducteurs pour l'Energétique (CRTSE),
Malika Berouaken
Centre de Recherche en Technologie des Semi-conducteurs pour l'Energétique (CRTSE),
Noureddine Gabouze
Centre de Recherche en Technologie des Semi-conducteurs pour l'Energétique (CRTSE),

Research Article

Keywords: Zinc oxide, ZnO, silicon type n, DRX, SEM, Angle contact, Electrodeposition, inter planar spacing, volume of the unit cell, micro strain, crystallinity

Posted Date: October 28th, 2021

DOI: https://doi.org/10.21203/rs.3.rs-1017928/v1

Abstract

In this work, thins films of zinc oxide were deposited on n-type silicon substrates by chemical electrodeposition. The effect of annealing temperature from 200 ° C to 600 ° C, with a step of 100 ° C, on the structural and morphological properties of ZnO layers has been studied. Scanning electron microscopy (SEM), X-ray diffraction (XRD) and contact angle measurements were used to characterize the morphology and structure of ZnO without and with annealing. The XRD patterns of unannealed ZnO thins films indicate the presence of three intense peaks along (100), (002) and (101) planes, while for the annealed ZnO layers the XRD patterns show also the three major peaks but the intensity of these peaks is increased except for a temperature of 600 ° C where is decreased. The comparison of the XRD patterns of the ZnO layers without and with annealing, reveal a shift in the 2θ diffraction angle, the calculation of the crystallinity confirms the obtained results. The contact angle measurements indicate that the ZnO layers without and with annealing at 200 °C are hydrophobic, the surface of the ZnO layer becomes hydrophilic at annealing temperatures exceeding 300 ° C. Finally, SEM images show the change in structure from a sand rose shape to a granular structure, confirming the XRD and contact angle results.

Introduction

In recent years, much researches have been carried out on different semiconductors, including zinc oxide (ZnO) which has a band gap of 3.37ev, with a high exciton binding energy (60 meV) [1]. Zinc oxide has attracted a great attention of many scientists and researchers for its different advantages such as its structural and morphological properties, its non-toxicity and its abundance of its components, its physical and chemical stability, its biocompatibility, high photosensitivity, piezoelectric and pyroelectric properties [2-4]. Because of its exceptional properties the ZnO has been exploited in various applications, including light emitting diodes, field effect transistors, gas sensors, and super capacitor, photovoltaic cells, etc [5-6]. There are many methods of elaborations of thin film of ZnO, two main ways can be noted: the physical way, such as sputtering, deposition by evaporation, growth by molecular jets, laser ablations, the methods consist in making the films from the material coming from a target [7]. However, these methods present several disadvantages such as they require very heavy equipment and very particular working conditions for example; vacuum, temperature, etc [8]. Unlike the chemical process, which consists in developing the film by chemical reaction or decompositions of a molecule, such as chemical vapor deposition CVD, spreading by centrifugation (spin coating), sol-gel method, spray pyrolysis method, or the electrodeposition method [9] [10], which has been chosen in this work. Thin films of ZnO can be deposited from the latter, using a rich solution of Zn^{2+} ions in an oxygen-rich medium, in our case, we choose hydrated hexa zinc nitrate as the source of Zn^{2+} ions, and potassium nitrate as supporting electrolyte [11-12]. Different researchers have studied the effect of the annealing temperature on the different properties of ZnO, such as morphology and structure [13-14]. Recently A. Al Zahrani and A. Zianal have studied this effect [15] by increasing the temperature from 300 ° C to 450 ° C with a step of 50 ° C. The obtained results indicate a decrease in particle size from 108.5 nm to 107.5 nm with an increase in the crystallite size from 17.41 to 19.51 nm. In this work, the effect of the annealing

temperature (from 200° C to 600 ° C) on different parameters such as inter-planar spacing, cell volume, dislocation density, the micro strain, and the crystallite size has been studied. The structure and morphology of ZnO thin films upon annealing temperature was investigated using X-ray diffractometry (XRD) and SEM scanning electron microscopy technique, supported by surface characterization by measuring the contact angle.

Experimental Procedure

2.1- Chemicals

The chemicals used in preparing the solutions consisted in zinc nitrate hexahydrate ($Zn(NO_3)_2$-$6H_2O$, SIGMA-ALDRICH, 98%, 297.5105g/mol), potassium nitrate (KNO_3, LABOSI, 99%, M=101.11g/mol). N-type silicon (CZ) oriented (100) ± 0.5° with a resistivity between [0,007-0.013] Ωcm, and thickness between [275-325 µm]. The chemicals products used for cleaning silicon are, trichlorethylene (C_2HCl_3, Prolabo, 99%, M=131,39 g/mol), acetone (C_3H_6O, Chemopharma,99.78%, M=50.08g/mol), ethanol (C_2H_5OH, Chemopharma,95%, M=46.07g/mol), acide Fluorohydrique (HF, Chemopharma,10%, M=20.0063g/mol).

2.2- Electrodeposition of ZnO thins films

Zinc oxide layers were electrochemically deposited on n-type Si substrate using the chronoamperometry method. First, the silicon wafers are cut with a diamond point into small silicon substrates of 1.5 cm x 1.5 cm, and then rinsed in three ultrasonic baths. The first one contains the tricloro-amine heated at 60 ° C during 20 minutes, after that the substrates are successively heated in acetone and ethanol at 55 ° C during 10 minutes, finally the wafers were rinsed in DI water and dried with nitrogen gas flow. The anodic electrodeposition of the ZnO layers was performed by using a simple electrochemical technique with a conventional three-electrode system, where the reference electrode was Ag/AgCl, the counter electrode was Platinum and n-Si substrates as the working electrode. Before each electrodeposition, the silicon substrates were dipped in hydrofluoric acid (10%) in order to remove the native oxide layer from the surface. The solution used was containing 6.10^{-3} M zinc nitrate hexahydrate $Zn(NO_3)_2$- $6H_2O$, and 1.10^{-1} M potassium nitrate KNO_3 which was prepared by using deionized water (EDI). The temperature was kept at 68 ° C during the electrodeposition and the deposition time was 30 min. for all experiments. An Autolab 128N potentiostat-galvanostat was used with a NOVA 1.8 control software.

The electrochemical synthesis of ZnO was carried out mainly by the method of raising the local pH, at the level of the working electrode, as cited by Peulon et al. [16]. According to several articles, the electrochemical formation mechanism of ZnO is initiated by the reduction of nitrate ions that produces hydroxide ions, followed by the precipitation of Zn(OH)2 [11,17,18]. If the temperature is sufficiently high (68 ° C in our study), this hydroxide dihydrates to form zinc II oxide (reaction 3) [12,18]. The sequence of the ZnO deposition can be summarized by the following equations [19,20]:

$NO_3^- + H_2O + 2\ e^- \rightarrow NO_2^- + 2\ OH^-$ (1)

$Zn^{2+} + 2\ OH^- \rightarrow Zn(OH)_2$ (2)

$Zn(OH)_2 \rightarrow ZnO + H_2O$ (3)

In order to define the polarization voltage for the ZnO electrodeposition, a cyclic voltammetry has been performed. Figure 1 shows cyclic voltammetry in a potential range from + 0,5 to -1,6 V with respect to Ag / AgCl at a scan rate of 10 mV s^{-1}. During the return sweep we note the existence of a peak around -1,2V which corresponds to the formation of ZnO [21], during the reverse scan direction no peak has been detected suggesting the absence of metallic zinc [22]. The results indicate that the applied voltage for the ZnO plating should be around -1.2V according to several works [9,19, 21,].

2.3-Materials characterization

In order to study the effect of the annealing temperature on the structural properties of thin zinc oxide, we used an X-ray diffractometer (XRD, Ultima IV, Itm2036E302) with radiation λCuKa = 1.54059A °, the voltage generator and tube current were (40kV, 40mA). The slew rate was 5,000 deg / min with a step of 0.05 °, the samples were scanned from 30 to 80 °. The contact angle measurements were carried out using a DGIDROP (GBX), using 3 µl drops of EDI deionized water deposited on the substrate. The system has built-in digital camera controlled using standard Visiodrop software. The morphologies of the obtained films have been investigated using an electron microscope JEOL JSM-6360 LV.

Results And Discussions

XRD patterns of the ZnO layer deposited without annealing are shown in Fig. 2, with the use of the PDXL2 software provided with the database (PDF-2, release 2014, 01 -073-8765). As it can be seen from the identification bars superimposed on the peaks 31.7 °, 34.35 °, 36.19 °, 47.55 °, 56.57 °, 62.74 °, 67.73 ° which gives us a structure of ZnO zincite (hexagonal phase, space group P63mc (186)) with mesh parameters a = b = 3.254167 A ° c = 5.216132 A °; c = 5.216132 A °. The XRD patterns obtained show that the deposited ZnO layer tends to present a preferential orientation (002) with the c axis perpendicular to the substrate [23]. These results are confirmed by several works [12, 24, 25].

The value of crystalline size D can be calculated using Scherer's equation (1), where K = 0.9 is the Scherer constant, λ = 0.15406 nm is the wavelength, θ is the peak position and the angle of Bragg diffraction in radians, and β full width at half maximum (FWHM) in radians [15].

$$D = \frac{K\lambda}{\beta cos\theta} \quad \text{..... (1)}$$

The inter-planar spacing d_{hkl} was calculated using the Bragg law relation (2), where n = 1 corresponds to the diffraction order, λ = 1.5406 A ° is the wavelength of the X-ray, and θ is the diffraction angle in radians

[26].

$$d_{hkl} = \frac{n\lambda}{2\sin\theta} \quad \text{..... (2)}$$

The volume of the unit cell V of the ZnO layer without annealing temperature was estimated by using equation (3) [27], such that a = b = 3.254167 A °, c = 5.216132 A ° extracted directly from the PDXL2 software. The dislocation density Φ in nm^{-2} and micro strain ξ are also calculated using the relation (4) and (5) [18, 28].

$$V = \sqrt{\frac{3}{2}}\, a^2\, C \quad \text{..... (3)}$$

$$\Phi = \frac{1}{D^2} \quad \text{..... (4)}$$

$$D = \frac{K\lambda}{\beta cos\theta} \quad \text{..... (5)}$$

In table 1 we summarize the mean crystalline size D, inter-planer spacing, unit cell volume, dislocation, and the micro strain.

The control of the annealing temperature after the deposition of ZnO is very important to obtain a good crystallinity. The XRD patterns of ZnO films grown at different annealing temperatures from 200 ° C to 600 ° C with steps of 100 ° C , compared to that the ZnO layer without annealing are shown in Fig 3 (a). XRD patterns exhibited three intense peaks with reflections from Bragg's angles at ~ 31.7 °, 34.3 °, 36.2 ° which correspond to the hexagonal phase of ZnO lattice planes of orientations (100), (002), (101), respectively. The diffraction reflections observed turned out to be well suited to the database (PDF-2, release 2014, 01-073-8765). In addition, these results show that the deposited ZnO layers are oriented towards the C (002) axis [23]. As the annealing temperature increased to 500 ° C, the intensity of the peaks at 31.7 °, 34.3 °, 36.2 ° became higher and sharper, indicating a good growth and crystallinity of the ZnO thin films. The high peak intensity corresponds to the annealing temperature of 500 ° C especially for the peak at ~ 34 °, on the contrary, for a temperature of 600 ° C the intensity of the peaks at 31.7 °, 34.3 °, 36.2 ° is reduced, while the intensity of the peak at 69 ° is increased. The database indicates the absence of metallic Zn phases or impurity phases, which indicates the formation of pure crystalline ZnO films. Figure 3 (b) reveals that the peak positions for the (100), (002) and (101) orientations of the ZnO films annealed at 300 ° C to 600 ° C were slightly shifted to higher 2θ values, revealing that a better crystallinity is obtained, result in good agreement with that obtained by M. Shaban et M. Zayed [27].

The inter-planar spacing, the dislocation density and the unit cell volume of ZnO films at different annealing temperatures were calculated by using successively the relations (2), (4), (3), the obtained results are shown in Table 2. The unit cell volume value is found about the same for unannealed and

annealed ZnO samples (see table 1 and 2), dislocation density is found 0.144 nm^{-2} for ZnO without annealing and even for films annealed at 200 ° C up to 500 ° C, on the other hand the dislocation density increases from 0.144 nm-1 for 200°C to 0.49 nm^{-1} when the temperature increases to 600 ° C. Moreover, the inter planer spacing is also fairly the same (2.62 ~ 2.63) for temperature up to 500 ° C but it changes at 600 ° C and takes a value of 1.41 A°.

The micro strain ξ and the crystalline size D were calculated by the relation (1) and (5), and represented in Figure 4. The micro strain is slightly reduced from 6,76 $.10^{-3}$ at ambient temperature to 5,32 $.10^{-3}$ at temperature of 600 ° C. The crystal size of ZnO grains is increased from 18 nm at ambient temperature to 20,17 nm at 400 ° C, and takes a low value at 600 ° C (11.97nm) which indicates that the best annealing temperature is obtained at 400 ° C.

Figs. 5 (a, b, c, d, e, f) show the SEM image of the surface morphology of ZnO layers electrochemically deposited without annealing and with annealing from 200 ° C to 600 ° C with steps of 100 ° C, respectively. Figs.5 (a) and (b) show that the surface of silicon substrate is densely and homogeneously covered with ZnO deposit. The latter appears as clusters in the form of sand roses containing micro-pillars of hexagonal shape oriented perpendicularly to the surface as shown in the magnification inset Fig.5a.This result was obtained by several authors [17, 9]. In addition, inset of Fig.5(a) shows the heads of the micro pillars are pointed, and have an average diameter of 0, 46 µm. Above the annealing temperature of 200 ° C, Fig.5(b), the diameter of the micro pillars increased to 0.84 µm, and the heads became porous, the average diameter of the pore is about 80,72 nm. With increasing the annealing temperature (T> 200 ° C) the structure changes completely from a sand rose form to a granular structure, at 300 ° C (Fig.5 (C)), the grains are aggregated with a random distribution in all directions. Switching to image of Fig.5(d), corresponding to an annealing temperature of 400 ° C, the aggregates become larger and randomly and sparsely distributed with different sizes. By tuning to 500 ° C, Fig.5 (e), the deposit appears densely distributed on the surface compared with that obtained for the substrate annealed at 400 ° C, that the deposited ZnO surface becomes rougher. The last image (Fig.5(f)) shows very sparse and sparse aggregate of ZnO grains. It is clear from these results that the uniformity, distribution, morphology and crystallinity of the deposits depends on the annealing temperatures.

Contact angle measurements are frequently used to study porosity, texturing, and treatment effects on the surface [28], in our case; we studied the effects of annealing temperature on the ZnO surface. A drop of 3µl of ultra-pure deionized water (DI) is used to perform these measurements at room temperature. First, we performed the measurement on the ZnO layer without annealing ,where a contact angle value of 122,1 ° (Fig.6a) is obtained, annealing of the deposit at 200 ° C gives a contact angle value of 100 ° (Fig.6b), a value greater than 90, which confirms the hydrophobicity of the ZnO surface [29].It is known that DI is a very polar medium with a very high surface energy, which could indicates that the zinc oxide surface is nonpolar with a very low surface energy leading to the formation of the beads in contact with the surface of ZnO (Fig. 6).

The variation of the contact angle upon different annealing temperature is represented in Figure 7. A decrease in the contact angle value from 122.1° without annealing to 29.5° is observed after successive annealing temperature from 200 ° C to 600 ° C indicating that the surface becomes hydrophilic. In addition, this confirms the transformation of ZnO bonds into polar bonds and the decrease in surface energy.

Conclusion

ZnO thin films have been successfully elaborated by electrodeposition method on silicon substrates. In this present work, we have based our study on the effect of annealing temperature on the morphology and structure of ZnO layers. The results showed that by increasing the temperature up to 500 ° C the crystallinity is also increased and a maximum crystal size of ZnO grains of 20 nm is obtained, on the other hand the micro strain is reduced, also is seen that the inter planar spacing, the density of dislocation and cell volume are the same for all temperatures except for 600 ° C. The contact angle measurements revealed to us that the deposited ZnO layer is hydrophobic at temperatures below 200 ° C. SEM images showed that the ZnO deposit exhibited sand-rose structure at temperatures below 200 ° C, while at temperatures higher, the structure becomes granular and textured, we deduce that the annealing temperature provides an average of controlled surface, structure and morphology of zinc oxide films.

References

1. Sana Akir, Alexandre Barras, Yannick Coffinier, Mohamed Bououdina, Rabah Boukherroub, Amel Dakhlaoui Omrani, Eco-friendly synthesis of ZnO nanoparticles with different morphologies and their visible light photocatalytic performance for the degradation of Rhodamine B, Ceramics International, 42 (2016) 10259-10265.
2. F. Barka-Bouaifel, B. Sieber, N. Bezzi, J.Benner, P.Roussel, L. Boussekey, S. Szunerits, R. Boukherroub, Synthesis and photocatalytic activity of iodine-doped ZnO nanoflowers, Journal of Material Chemistry, 21 (2011) 10982–10989.
3. A. Taabouche, A. Bouabellou, F. Kermiche, F. Hanini, C. Sedrati, Y. Bouachiba, C. Benazzouz, Preparation and characterization of Al-doped ZnO piezoelectric thin films grown by pulsed laser deposition, Ceramics International, 42 (2016), Issue 6,
4. Bilgin, V., Sarica, E., Demirselcuk, B. et al. Iron doped ZnO thin films deposited by ultrasonic spray pyrolysis: structural, morphological, optical, electrical and magnetic investigations. J Mater Sci: Mater Electron, 29(2018), 17542–17551.
5. Badis Rahal, Boubekeur Boudine, Nassim Souami, Menouar Siad, Miloud Sebais, Ouahiba Halimi, Lakhdar Guerbous, Behavior Study of the Nanostructured Zn1-xCdxO ($0 \leq x \leq 0.1$) Semiconductor Thin Films Deposited onto Silicon Substrate by Dip-Coating Method,
6. Sun L, He H, Liu C, Lu Y, Ye Z, controllable growth and optical properties of ZnO nanostructures on Si nanowire arrays, Cryst Eng Comm, (2011). 13:2439

7. Huang, Z.-H., Song, Y., Feng, D.-Y., Sun, Z., Sun, X., & Liu, X.-X. (2018). High Mass Loading MnO2 with Hierarchical Nanostructures for Supercapacitors. ACS Nano, 12(4), 3557–3567.
8. Tynell, T, & Karppinen, M, Atomic layer deposition of ZnO: a review, Semiconductor Science and Technology, 29(2014), 043001.
9. N. Ait Ahmed, G. Fortas, H. Hammache, S. Sam, A. Keffous, A. Manseri, L. Guerbous, N. Gabouze, Structural and morphological study of ZnO thin films electrodeposited on n-type silicon, Applied Surface Science, Volume 256, Issue 24, (2010), 7442-7445,
10. Peulon. S, Lincot. D, Cathodic electrodeposition from aqueous solution of dense or open-structured zinc oxide films, Advanced Materials, 8 (1996) 166–170.
11. Mahmoud Abdelfatah, H.Y. Salah, M.I. EL-Henawey, A.H. Oraby, Abdelhamid El-Shaer, Walid Ismail, Insight into Co concentrations effect on the structural, optical, and photoelectrochemical properties of ZnO rod arrays for optoelectronic applications, Journal of Alloys and Compounds, 873 (2021), 159875.
12. Arslan A, Hür E, Ilican S, Caglar Y, Caglar M. Controlled growth of c-axis oriented ZnO nanorod array films by electrodeposition method and characterization. Spectrochim Acta A Mol Biomol Spectrosc. 15(2014), 716-23
13. S. Paiman, T. Hui Ling, M. Husham, Suresh Sagadevan, Significant effect on annealing temperature and enhancement on structural, optical and electrical properties of zinc oxide nanowires, Results in Physics, 17(2020), 2211-3797
14. M. M. Kareem, Z. T. Khodair, F. Y. Mohammed, Effect of annealing temperature on Structural, morphological and optical properties of ZnO nanorod thin films prepared by hydrothermal method, J. of Ovonic Research, 16(2020) 53-61.
15. Al-Zahrani, A. A., Zainal, Z., Talib, Z. A., Lim, H. N., Fudzi, L. M., Holi, A. M., & Mohd Ali, M. S, Effect of Annealing Temperature on the Performance of ZnO Seed Layer for Photoanode in Photoelectrochemical Cells, Defect and Diffusion Forum, 398(2020), 156–166.
16. Peulon, S. Mechanistic Study of Cathodic Electrodeposition of Zinc Oxide and Zinc Hydroxychloride Films from Oxygenated Aqueous Zinc Chloride Solutions. Journal of The Electrochemical Society. (1998), 145(3), 864.
17. Shaolin Yang, Simiao Sha, Hui Lu, Jiandong Wu, Jinfu Ma, Dewei Wang, Zhiling Sheng, Electrodeposition of hierarchical zinc oxide nanostructures on metal meshes as photoanodes for flexible dye-sensitized solar cells, Colloids and Surfaces A: Physicochemical and Engineering Aspects, 594 (2020), 0927-7757.
18. K. Deva Arun Kumar, V. Ganesh, S. Valanarasu, Mohd Shkir, I. Kulandaisamy, A. Kathalingam, S. AlFaify, Effect of solvent on the key properties of Al doped ZnO films prepared by nebulized spray pyrolysis technique, Materials Chemistry and Physics, 212 (2018), 167-174.
19. T. Mahalingam, V.S. John, M. Raja, Y.K. Su, P.J. Sebastian, Electrodeposition and characterization of transparent ZnO thin films, Solar Energy Materials and Solar Cells, 88 (2005), 227-235.

20. Kara, R., Mentar, L., & Azizi, A.. Synthesis and characterization of Mg-doped ZnO thin-films electrochemically grown on FTO substrates for optoelectronic applications. RSC Advances, 10 (2020), 40467–40479.
21. Baka, O, Azizi, A., Velumani, S. et al. Effect of Al concentrations on the electrodeposition and properties of transparent Al-doped ZnO thin films. J Mater Sci: Mater Electron, 25 (2014) , 1761–1769.
22. Marianna Kemell, Frédéric Dartigues, Mikko Ritala, Markku Leskelä, Electrochemical preparation of In and Al doped ZnO thin films for CuInSe2 solar cells, Thin Solid Films, 434 (2003), 20-23.
23. Weon Cheol Lim, Jitendra Pal Singh, Younghak Kim, Jonghan Song, Keun Hwa Chae, Tae-Yeon Seong, Effect of thermal annealing on the properties of ZnO thin films, Vacuum, 183 (2021), 109776.
24. Nuruddin, A., Yuliarto, B., Kurniasih, S., Setiyanto, H., & Ramelan, A, Preparation Of Superhydrophobic Zinc Oxide Nanorods Coating On Stainless Steel Via Chemical Bath Deposition. IOP Conference Series: Materials Science and Engineering, 547 (2019), 012052.
25. Kaushlya Sihag, Nitika Choudhary, Effect of annealing temperature on phase and morphology of zinc oxide nanostructures with dielectric studies, Materials Today: Proceedings, 28 (2020), 298-301.
26. Praloy Mondal, Effect of Oxygen vacancy induced defect on the optical emission and excitonic lifetime of intrinsic ZnO, Optical Materials, 98 (2019), 109476.
27. Shaban, M., Zayed, M., & Hamdy, H, Nanostructured ZnO thin films for self-cleaning applications. RSC Advances, 7(2017), 617–631.
28. Kahina Lasmi, Habiba Derder, Amina Kermad, Sabrina Sam, Hinda Boukhalfa-Abib, Samia Belhousse, Fatma Zohra Tighilt, Khaled Hamdani, Noureddine Gabouze, Tyrosinase immobilization on functionalized porous silicon surface for optical monitoring of pyrocatechol, Applied Surface Science, 446 (2018), 3-9.
29. Ghannam, H., Chahboun, A., & Turmine, M. Wettability of zinc oxide nanorod surfaces. RSC Advances, 9(2019), 38289–38297.

Tables

Table 1: Lattice parameters (a,b & c), crystalline size (D), volume (V), dislocation density (Φ), and micro strain (ξ) of the thins film of ZnO without annealing.

Temperature	crystallite size (nm)	Inter planar spacing (dhkl) Å°	lattice parameters Å a=b c	Cell Volume (V) $A^{\circ 3}$	Dislocation density (Φ) nm^{-2}	Micro strain x 10^3 (ξ)
Ambiant	17,847	2,634	3.254167 5.216132	47,83644	0,1441	6,769

Table 2: Inter planar spacing (dhkl) A°, Cell Volume (V) $A^{\circ 3}$, dislocation density (Φ) nm^{-2} of the thins film of ZnO at room temperature and different annealing temperature .

Température	Intera planar spacing (dhkl) Å°	Cell Volume (V) $A^{\circ 3}$	Dislocation density (Φ) nm^{-2}
200°C	2,633	47,767	0,144
300°C	2,631	47,572	0,144
400°C	2,630	47,836	0,144
500°C	2,626	47,666	0,144

Figures

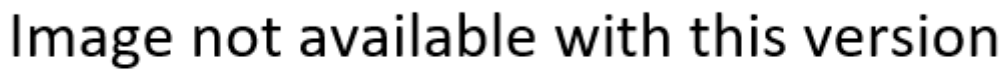

Figure 1

Cyclic voltammogram obtained on an n-type silicon electrode (100) in an aqueous solution of [Zn2+] = 6.10-3 M with a scan rate of 10 mV s−1.

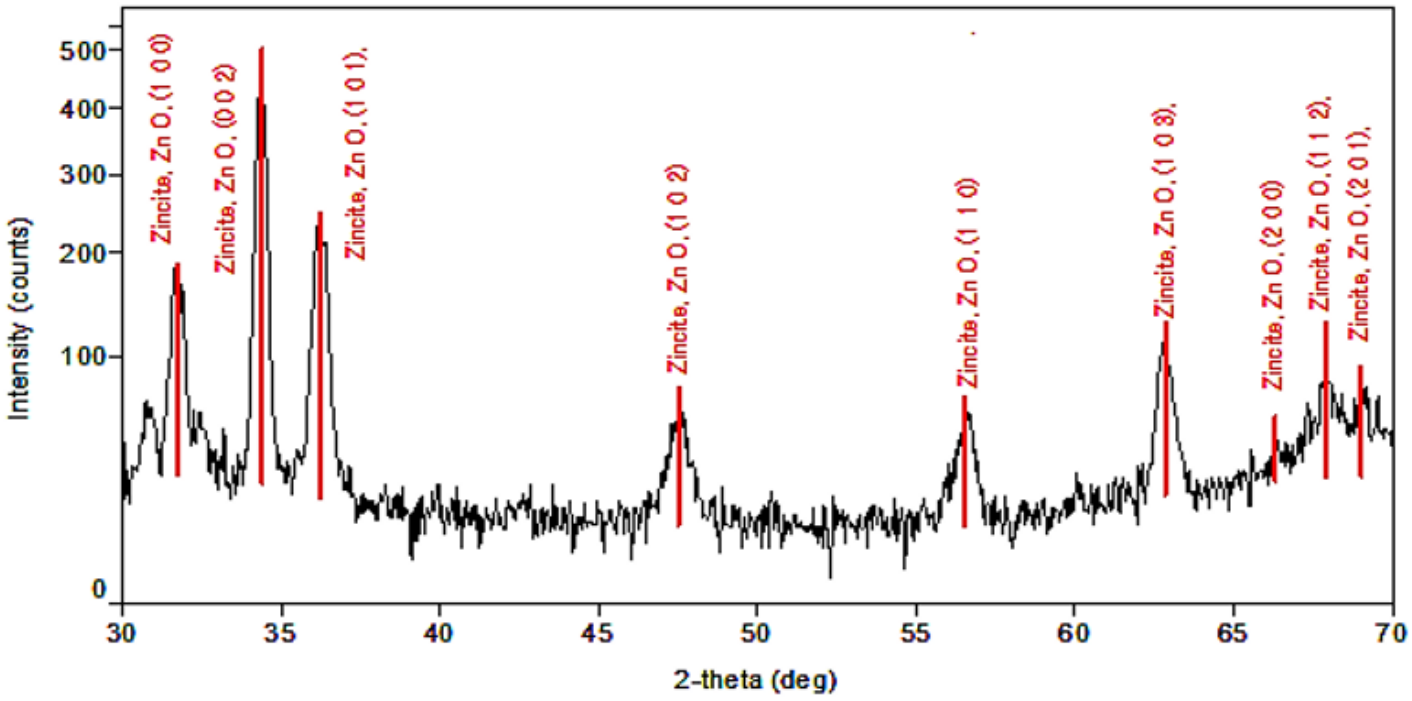

Figure 2

XRD patterns of ZnO without annealing temperature.

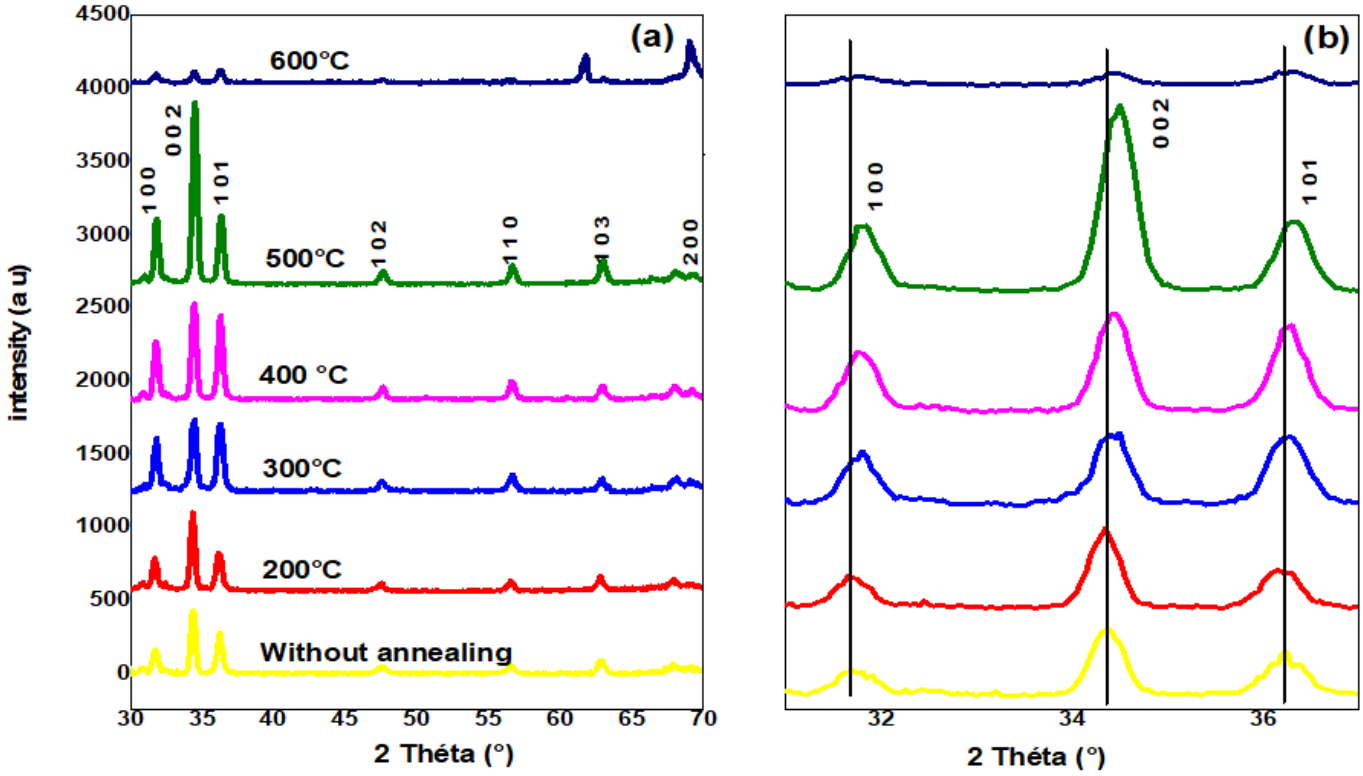

Figure 3

(a) XRD patterns of ZnO without annealing and (b) annealed at 200, 300, 400, 500, 600°C, (b) comparison of peak angle value as a function of annealing temperatures.

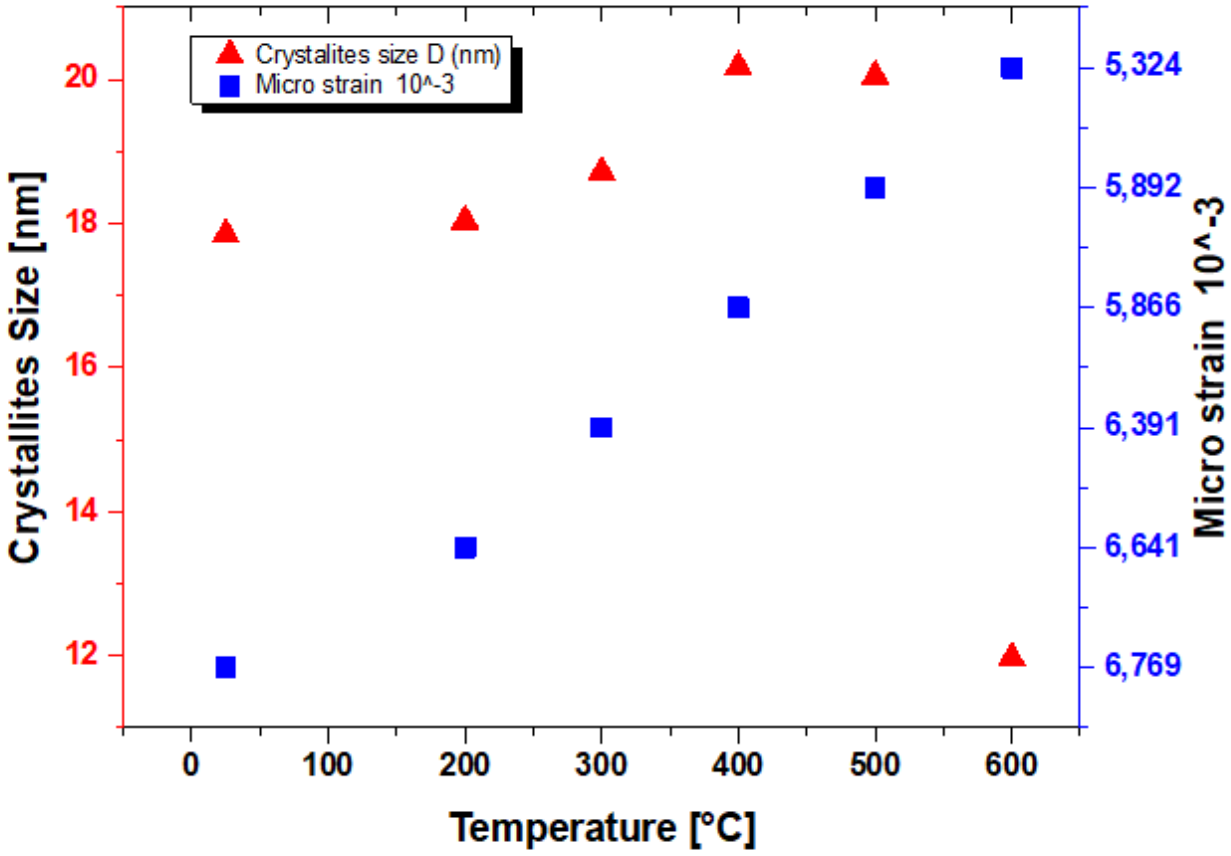

Figure 4

crystallite size and micro strain as a function of annealing temperature.

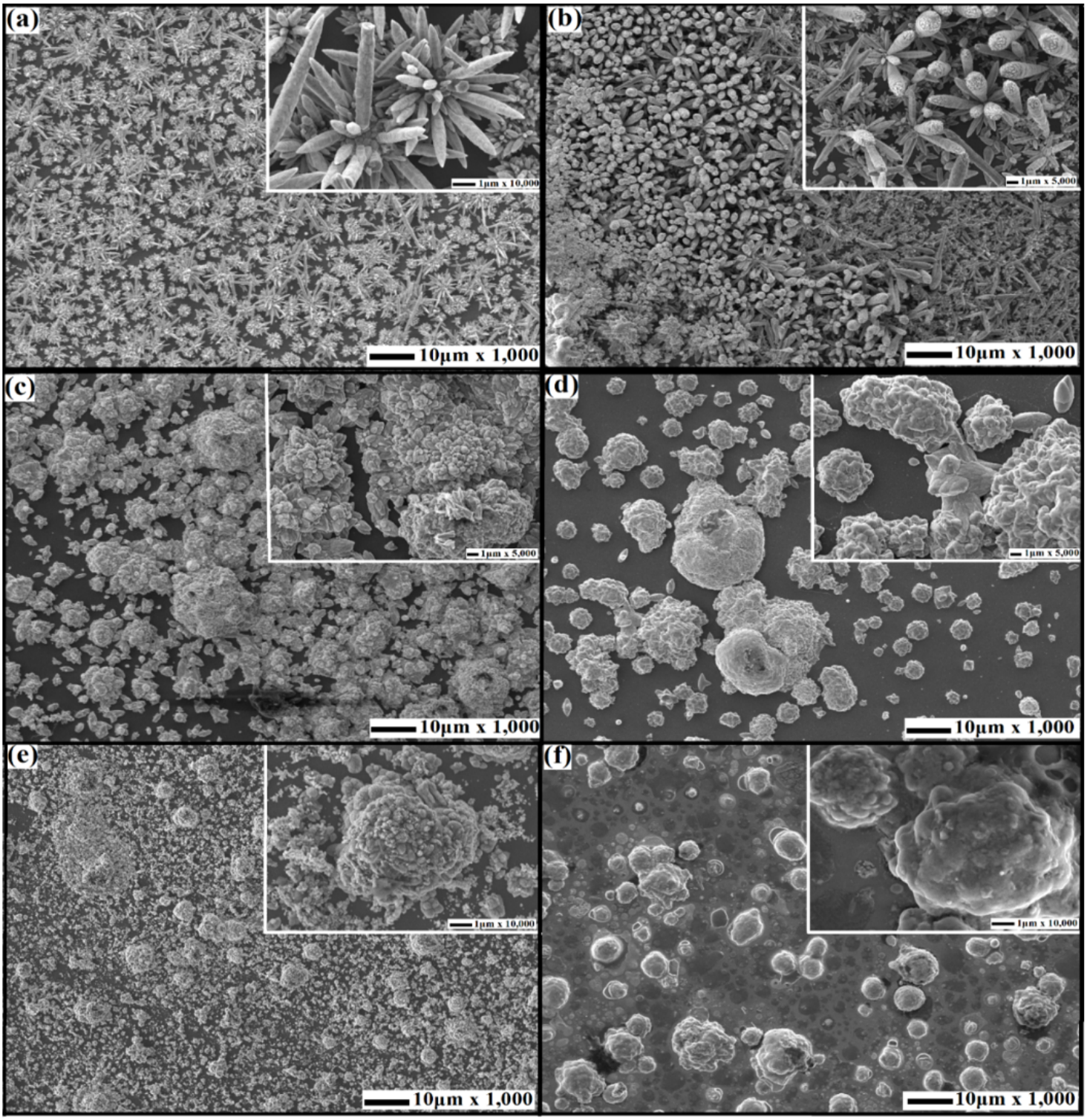

Figure 5

SEM images of ZnO thin films without annealing (a) and treating with annealing from 200 ° C to 600 ° C with steps of 100 ° C (b, c, d, e, f).

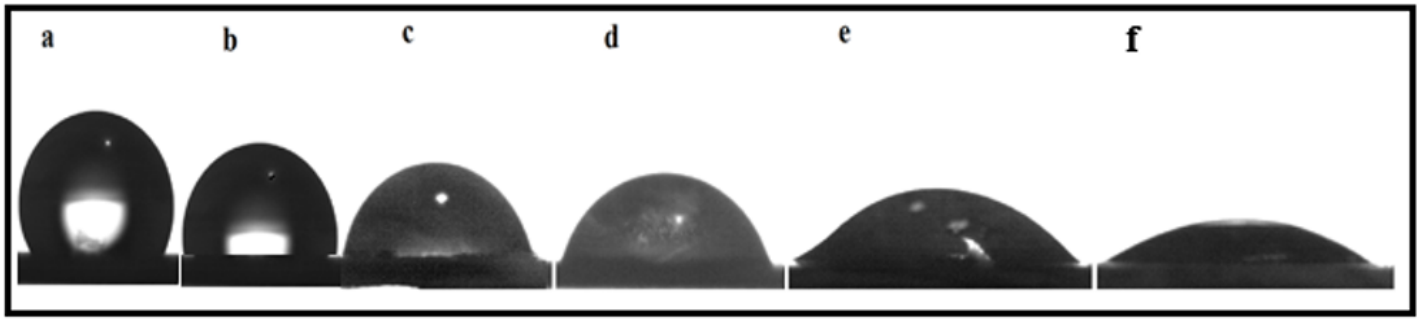

Figure 6

ZnO contact angle image (a) without annealing, and with annealing at (b) 200 °C, (c) 300 °C, (d) 400 °C, (e) 500°C, (f) 600°C.

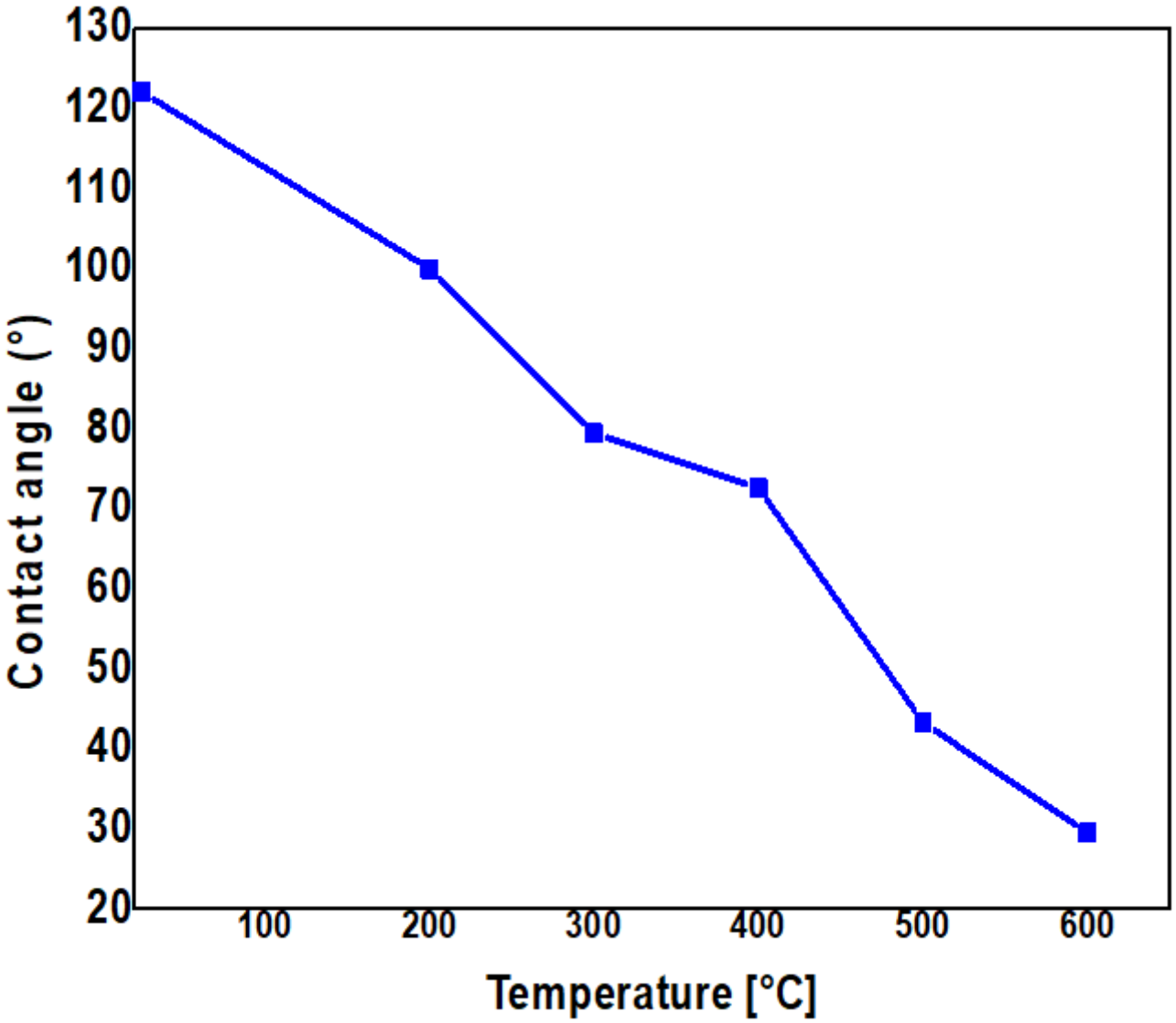

Figure 7

The contact angle of ZnO without annealing, and with annealing to 200 °C up to 600 °C with a step of 100 °C.